GEOPHYSICAL RESEARCH LETTERS, VOL. 40, 1–6, doi:10.1002/grl.50257, 2013

Broadband array observations of the 300 km seismic discontinuity

Nicholas C. Schmerr,[1] Byron M. Kelly,[2] and Michael S. Thorne[3]

Received 3 January 2013; revised 11 February 2013; accepted 13 February 2013.

[1] Intermittent seismic discontinuities near 250–300 km depth beneath South America and the Pacific basin are detected with high-resolution seismic array methods that use SS and PP precursors recorded at the High Lava Plains Seismic Experiment and the EarthScope Transportable Array. The transformation of coesite to stishovite in an eclogite-rich mantle composition produces a seismic discontinuity near 300 km depth; lateral changes in basalt fraction of the upper mantle will thus produce an intermittent seismic discontinuity. The sensitivity of the precursors to intermittent seismic structure is addressed using an axisymmetric finite difference model of wave propagation in the mantle. These numerical experiments find that the precursors are sensitive to structures ≥500 km in lateral extent and that the observations of this discontinuity are plausibly tied to lateral variations in basaltic composition of the upper mantle related to dynamics, such as plumes and subduction. **Citation:** Schmerr, N. C., B. M. Kelly, and M. S. Thorne (2013), Broadband array observations of the 300 km seismic discontinuity, *Geophys. Res. Lett.*, *40*, doi:10.1002/grl.50257.

1. Introduction

[2] A variety of past studies have investigated the structure of seismic discontinuities that occur in the 250–350 km depth range in the Earth's upper mantle [e.g., *Bagley and Revenaugh*, 2008; *Deuss and Woodhouse*, 2002; *Revenaugh and Jordan*, 1991; *Wajeman*, 1988; *Williams and Revenaugh*, 2005; *Zhang and Lay*, 1993]. Previous seismic studies indicate that interfaces observed near these depths possess a relatively low shear impedance contrast (3%–5%) but are seismically sharp, with the gradient constrained to be <5 km across the discontinuity [*Bagley and Revenaugh*, 2008; *Revenaugh and Jordan*, 1991; *Zheng et al.*, 2007]. Seismic discontinuities near 300 km depth are primarily observed beneath regions of subduction [*Zhang and Lay*, 1993], continents [*Wajeman*, 1988], and a few hot spots [*Bagley et al.*, 2009; *Courtier et al.*, 2007] (Figure 1). Here, we used underside reflections of shear and compressional wave energy arriving as precursors to the seismic phases SS and PP to image the depth and sharpness of these shallow discontinuities. These precursors arrive as low amplitude energy (1%–10% of the SS or PP phase) several hundred seconds before the reference underside reflected seismic phase (SS or PP) and have been used extensively to map upper mantle discontinuity structure [see the review by: *Deuss*, 2009]. For simplicity, we referred to the average depth (300 km) to label these discontinuities, although the interfaces may occur at a slightly different depth in the Earth.

[3] Several different mineral physical and petrologic mechanisms have been proposed to explain the mantle discontinuities near 300 km depth [for a review, see *Williams and Revenaugh*, 2005]. Mechanisms ascribed to these boundaries include the formation of hydrous phase A in subduction zones [*Akaogi and Akimoto*, 1980; *Revenaugh and Jordan*, 1991], a crystallographic transition in pyroxene from orthorhombic to monoclinic structure [*Woodland*, 1998], and the solid-to-solid phase transformation of coesite to stishovite in subducted eclogitic materials [*Williams and Revenaugh*, 2005]. The formation of hydrous phase A is feasible in regions of subduction, although relatively low mantle temperatures are required to stabilize this seismic phase [*Revenaugh and Jordan*, 1991]. Similarly, the formation of stishovite requires the presence of unequilibrated basalt in the mantle [*Liu et al.*, 1996]. The crystallographic reorganization of pyroxene produces a 0.7% shear impedance contrast [*Woodland*, 1998], which is in poor agreement with the higher contrast detected in previous seismic observations. Thermodynamical modeling of whole mantle compositions for mechanically mixed and equilibrium assemblages of the mantle indicates the coesite to stishovite transformation may be present where grains of mid-ocean ridge basalt and harzburgite remain unequilibrated in the mantle [*Xu et al.*, 2008].

[4] In this article, we used underside reflected energy to investigate the depth, lateral extent, and sharpness of the 300 km interfaces. Where past work with SS and PP precursors combined data from numerous earthquakes recorded by seismic stations around the globe to stack and bring the precursory seismic phases out of the background seismic noise [e.g., *Deuss*, 2009], we used a three-dimensional broadband array methodology [*Rost and Thomas*, 2009] to analyze each earthquake independently, striving to maximize seismic energy from the precursory arrivals while eliminating energy from other seismic phases that may interfere with arrivals in the depth range of 250–350 km. We modeled our results using an axisymmetric finite difference wave propagation code [*Jahnke et al.*, 2008] that allows us to investigate the effects of lateral variations in seismic structure and to examine the expected response from small-scale intermittent seismic discontinuities. The resulting observations provide constraint on the scale of chemical and thermal anomalies within the upper mantle.

2. Data Set and Method

[5] We collected broadband displacement seismograms recorded from 2005 to 2009 by the EarthScope Transportable Array and the High Lava Plains Seismic Experiment

[1]NASA Goddard Space Flight Center, Planetary Geodynamics Laboratory, Greenbelt, Maryland, USA.
[2]Department of Geoscience, University of Calgary, Calgary, Alberta, Canada.
[3]Department of Geology and Geophysics, University of Utah, Salt Lake City, Utah, USA.

Corresponding author: N. C. Schmerr, NASA Goddard Space Flight Center, Planetary Geodynamics Laboratory, Code 698, Greenbelt, MD 20771, USA. (nicholas.c.schmerr@nasa.gov)

0094-8276/13/10.1002/grl.50257

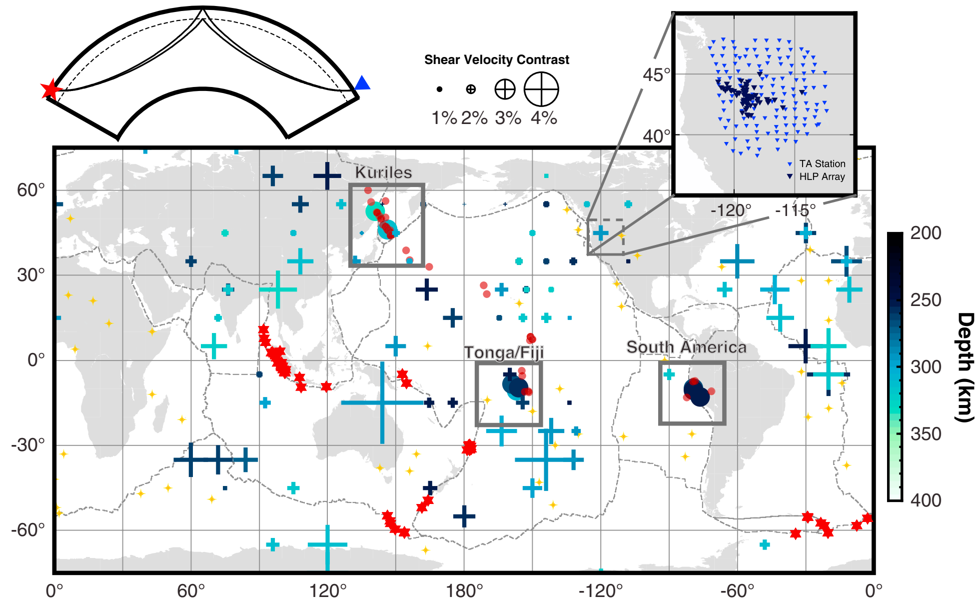

Figure 1. Depth and velocity contrasts of SS and PP precursor detections of the 300 km discontinuity. Raypath of surface reflection and precursory phase from source (red star) to seismometer (blue triangle) is in the upper left. The map shows the locations of detections of the 300 km discontinuity (colored circles), nondetections (red circles), and results from [*Deuss and Woodhouse*, 2002] (colored crosses). Detections are scaled by the size of the shear velocity contrast at the discontinuity. Hot spots (yellow stars) and plate boundaries (broken lines) indicate volcanic and tectonic features.

(HLP). The HLP stations were supplemented by transportable array stations deployed within 750 km from the center of the HLP. The instrument response was deconvolved from each seismogram, and the horizontal channels were rotated to obtain the transverse component of motion. Seismograms of each event were visually inspected to determine the quality of the body wave arrivals; highest quality events did not require any filtering to identify the SS or PP arrivals from the background noise. We retained earthquakes that possessed clear SS or PP arrivals when band-pass filtered at corners of 10–50 s. The data set initially consisted of 187 events ($M_W \geq 5.8$) and 25,340 seismograms; after visual inspection, we kept 36 high-quality events with 4046 seismograms, with an average of 112 records per event (minimum 15, maximum 231). We marked a reference time for the PP and SS arrivals using the travel time of the highest amplitude arrival of the first swing of the SS or PP waveform.

[6] To investigate discontinuity structure, we used two array methods, velocity spectral analysis (vespagram) and migration, to bring the precursor arrivals out of the noise levels. A fourth-root vespagram [*Davies et al.*, 1971] is generated for each event to verify the arrival times and slowness of precursors matched predictions from ak135 [*Kennett et al.*, 1995]. Only vespagrams with a high signal-to-noise ratio for SS or PP and precursors are kept for further analysis (Figure 2). We then retrieved the depths of the upper mantle discontinuities using a migration method adapted from [*Schmerr and Thomas*, 2011]. The migration method allows the back projection of precursory energy to the underside reflection point and lessens the size of the Fresnel zone, thereby enhancing resolution [*Rost and Thomas*, 2009]. To migrate, we generated a 40° × 40° grid in 1° increments every 5 km between 0 and 900 km depth. This grid is centered on the reflection point halfway between the average array center and the source location. Travel times are calculated between each grid point and array station, as well as between each grid point and source location by raytracing through model ak135. The seismic traces are shifted by the resulting delay times and stacked. We selected the maximum amplitude in a 3 s window centered on the theoretical arrival time of the precursor and used a bootstrap resampling algorithm with 300 random replacement resamples to evaluate the 95% confidence amplitude in migration grid point [*Efron and Tibshirani*, 1986]. The depth of the discontinuity is selected by taking an amplitude profile at the calculated reflection point for the source and array center (Figure 2). Ultimately, this migration technique removes the effects of seismic energy at other slowness levels and enhances the arrivals from the precursors [*Rost and Thomas*, 2009].

3. Results

[7] An event is considered suitable to search for a 300 km precursor if the data satisfy the following criteria: (1) the 410 km and 660 km precursors must all be present in both the vespagram and migration for the event, (2) the vespagram must indicate that the precursory energy is well separated in slowness from interfering seismic phases, such as ScS660ScS and PKIKP (Figure 2), and (3) the SS or PP signal-to-noise ratio must be ≥3.0. The SS data are band-pass filtered with corners at 0.067 and 0.020 Hz, whereas the PP data are filtered with corners at 0.010 and 0.020 Hz. Of the 187 events that satisfy our source parameters and these criteria, 36 were sufficient for further analysis.

[8] The depth of a discontinuity is determined using the migrated amplitude profile at the calculated reflection point for the source and array center. The migration grid allows us to resolve precursory depths with 5 km precision. We corrected depths using one-dimensional raytracing through CRUST 2.0 [*Bassin et al.*, 2000], the *P* wave tomography

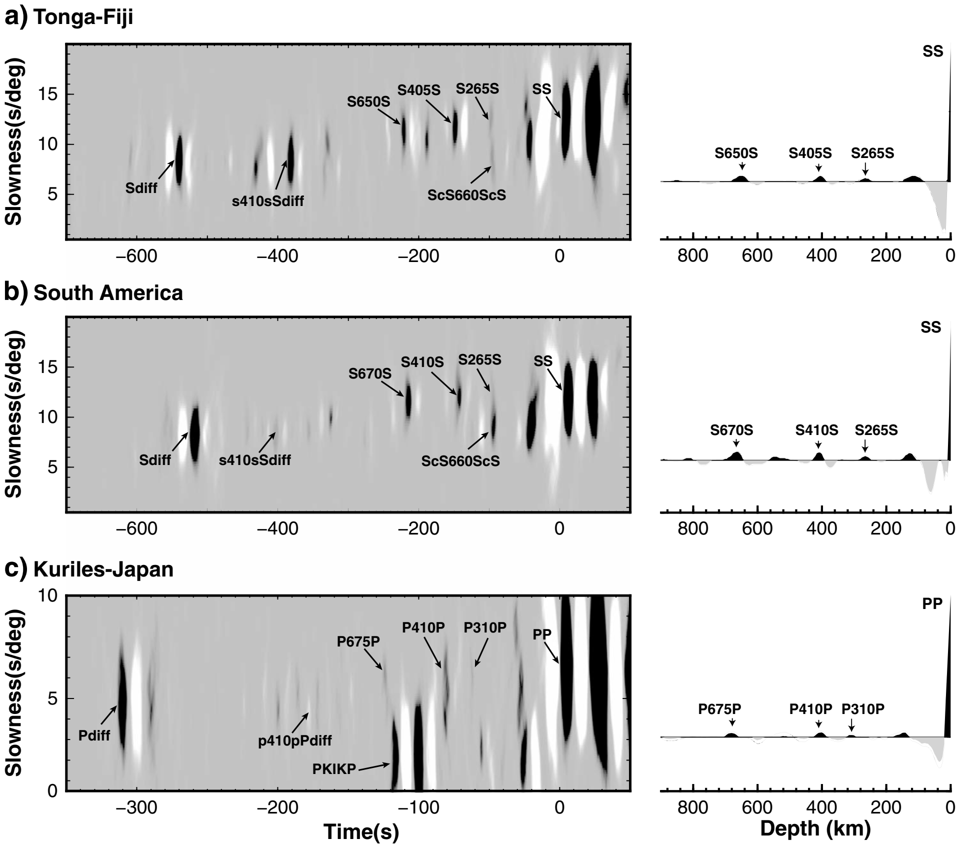

Figure 2. Vespagrams and migration amplitudes for example events with 300 km discontinuity detections. (a) SS results for event 2007 030 04:54:50, located at 146.30ºE, 54.74ºS, $M_W = 6.8$, and 11 km depth. (b) SS results for event 2008 054 15:57:19, located at 23.42ºE, 57.33ºS, $M_W = 6.7$, and 10 km depth. ScS660ScS extends slightly into the S265S slowness range; however, similar behavior at high slowness (>12 s/deg) is not observed for the s410sSdiff phase. (c) PP results for event 2008 056 18:06:03, located at 99.89ºE, 2.33ºS, $M_W = 6.6$, and 25 km depth. Vespagram amplitudes (positive—black; negative—white) are normalized to unity. The migration amplitudes are shown for the underside reflection point for the array center and source location. The 95% confident positive (black) and negative (gray) amplitudes are from the bootstrap resampling algorithm.

model MITP08 [*Li et al.*, 2008], and the *S* wave tomography model S40RTS [*Ritsema et al.*, 2011]. Of the events analyzed, 36 produced 410 and 660 km discontinuity related precursors. Of these 36 events, 11 events show precursory seismic phases from a discontinuity at 250–310 km depth in both the vespagrams and migrated seismic energy (Figure 1). Table 1 summarizes the average depths of each discontinuity in the regions where a 300 km discontinuity is detected, the corresponding seismic phase that produced the detection, and the average amplitude ratios of the precursor to the reference seismic phases. The amplitude ratio is defined as the maximum enveloped amplitude of the precursor to the reference SS or PP amplitude as measured from the migrated seismic energy. Precursor amplitude ratios are adjusted for the effects of source radiation pattern, geometric spreading, and differential attenuation using a correction factor computed from reflectivity synthetics [*Fuchs and Müller*, 1971]. There is a strong tradeoff in source radiation patterns for SS and PP precursory energy. An optimal radiation pattern for vertically polarized PP energy will minimize transversely polarized SS energy; thus, analyses for each event are limited to either SS or PP.

[9] Precursor amplitude ratios provide information on the velocity and density contrasts across the discontinuity [e.g., *Shearer and Flanagan*, 1999]. We obtained the density and *S* and *P* wave velocity contrasts at the 300 km discontinuity by forward modeling. The precursory waveshape is compared with a reflectivity synthetic calculated for a range of velocity and density contrasts (0%–10%) to provide an estimate for the elastic contrasts at the discontinuity.

Table 1. Regional averages of discontinuity depths and precursory amplitude ratios

Region	Center latitude (º)	Center Longitude (º)	Phase	d410 (km)	d660 (km)	d300 (km)	amp410 (2σ)	amp660 (2σ)	amp300 (2σ)
Kuriles-Japan	46.11	146.22	PP	413	673	310	0.031 (0.012)	0.023 (0.012)	0.022 (0.014)
Tonga-Fiji	−9.70	−156.93	SS	405	650	265	0.041 (0.009)	0.040 (0.009)	0.025 (0.010)
South America	−10.53	−79.30	SS	405	670	250	0.045 (0.007)	0.047 (0.008)	0.025 (0.006)

The migrated SS precursor amplitude ratios for Tonga-Fiji and South America are nearly identical (0.025); if we use the 300 km PP precursor amplitude ratio values from the Kurile subduction zone (0.022) as our *P* wave constraint, we obtain a *P* wave velocity contrast of 3.3% ± 1.8%, an *S* wave velocity contrast of 3.0% ± 1.1%, and a density contrast of 1.9% ± 1.2%. The corresponding shear impedance contrast is 4.7% ± 1.4%, and compressional impedance is 5.0% ± 1.6% and is agreement with a value of 5% reported in prior studies [e.g., *Bagley and Revenaugh*, 2008; *Courtier et al.*, 2007; *Revenaugh and Jordan*, 1991; *Zheng et al.*, 2007].

4. Discussion

[10] The regional detections of the 300 km discontinuity in this study overlap previous results from stacks of SS precursors in these regions [*Deuss and Woodhouse*, 2002]. Stacking approaches approximate the large Fresnel zone (>1000 km width) sensitivity of the SS and PP precursors [*Chaljub and Tarantola*, 1997], whereas array methods seek to increase the sensitivity to smaller-scale structure within the mantle [*Rost and Thomas*, 2009]. Six events sampling in the mid-Pacific near the Hawaiian-Emperor archipelago did not show evidence for a precursor near 300 km depth, although past studies closer to the hot spot [*Courtier et al.*, 2007; *Deuss and Woodhouse*, 2002] found a discontinuity near 250–300 km near the Hawaiian island chain (Figure 1). In all three study regions, there are events that generate a precursory arrival from the 300 km discontinuity that sample alongside events that did not produce a precursory arrival from the discontinuity. This is suggestive of a highly localized and regional discontinuity that is only illuminated when either source/station geometry is properly aligned or the regional structure is extensive enough to produce more than a specular reflection from the discontinuity. Small-scale scattering from near-source or near station heterogeneity can produce additional energy [*Zheng and Romanowicz*, 2012], but we can rule out such effects for our data set using slowness constraints provided by the vespagrams. Localized, large-scale topography may focus and defocus seismic waves and produce scattered arrivals [e.g., *Chaljub and Tarantola*, 1997]; however, detailed short-period modeling efforts of topographic effects are beyond the scope of this work and will be the topic of future investigations. Past efforts to resolve localized discontinuity structure with the SS and PP precursors were limited to relatively long period approaches (>30 s) [*Chaljub and Tarantola*, 1997; *Shearer et al.*, 1999]. We addressed the hypothesis that the 300 km discontinuity is a laterally intermittent seismic interface with synthetic modeling at periods down to 10 s.

[11] We computed synthetic seismograms using the 2.5-D axisymmetric finite difference technique SHaxi [*Jahnke et al.*, 2008]. This method computes the full SH wavefield for two-dimensional model geometries with correct three-dimensional geometrical spreading. In this study, we generated models with 20,000 lateral (0°–180° in the lateral direction) and 3800 vertical (surface to CMB) grid points. This discretization is chosen to provide 10 s dominant period synthetic seismograms for a 3000 s simulation at epicentral distances up to 130°. Overridden on the PREM [*Dziewonski and Anderson*, 1981] background model is a reflector with a laterally varying scale length (in the great circle arc direction) centered at an epicentral distance of 55° (Figure 3). A discontinuous impedance contrast is imposed at 275 km depth that linearly gradates back to PREM values at a depth of 415 km (see Figure 3a). We explored synthetic models with density increases of 1%, 3%, and 5% and *S* wave velocity increases of 1%, 2%, and 4%. Reflector lengths examined are 50, 100, 200, 300, 400, 500, 750, 1000, 2000, and 5000 km. We tested all combinations of these parameters, thus computing synthetics for 90 unique models, exploring shear impedance contrasts that range from 1% to 9%.

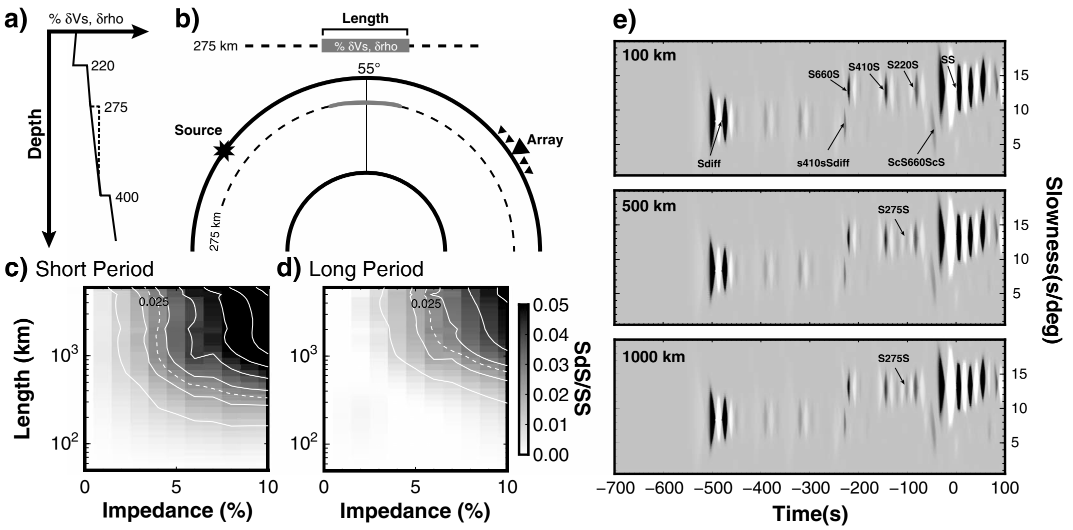

Figure 3. Detectability of the 300 km discontinuity from 2.5-D axisymmetric forward modeling. (a) Perturbation structure relative to the PREM background model. (b) Lateral variation of the 300 km discontinuity introduced in Figure 3a. (c) Migrated precursor amplitude ratios for a band-pass filter with corners at 0.1 and 0.02 Hz. Contour intervals are every 0.01 SdS/SS. (d) The same as Figure 3c, except for a band-pass filter with corners at 0.04 and 0.02 Hz. The labeled contour indicates the observed SS precursory amplitude ratio for the 300 km discontinuity in this study. (e) Example vespagrams from the forward modeling for a shear impedance contrast of 5%. Reflector lengths are given in the upper left of each panel.

[12] The resulting synthetics are migrated to obtain the depth and amplitude ratio of the S275S precursor. Figure 3c shows the results for the amplitude ratios for the S275S phase. At shorter periods (data band-pass filtered at 10–50 s), the expected precursory amplitude ratio of the 275 km discontinuity is recovered for structures 600–750 km wide and weakens for smaller-scale features. At longer periods (30–50 s), expected precursory amplitude ratios fall significantly for structures less than 1000 km in width. The modeling suggests discontinuity structure, especially at shorter periods, is (1) resolvable below the Fresnel zone with array detection techniques, (2) strongly affected by scattered waves and three-dimensional structure, and (3) likely underestimating the size of the associated impedance contrast for regional interfaces in the presence of small-scale structure. Thus, we concluded that the interface observed in our data set near 300 km depth represents a regional discontinuity on the order of 500 km, with an impedance contrast of 4%–5% or greater.

[13] Mechanisms that would generate such small-scale variations in mantle structure possessing large impedance contrasts include the presence of eclogitic materials or hydration of mantle materials [*Xu et al.*, 2008]. Previous studies have suggested that the 300 km discontinuity is associated with the transition of coesite to stishovite, for eclogitic materials with 4%–10% SiO_2 [*Williams and Revenaugh*, 2005]. Eclogitic materials in the upper mantle are likely remnant crust, consisting primarily of subducted mid-ocean ridge basalt. The impedance contrast of the coesite to stishovite phase transition for thermodynamical models of primarily basaltic materials is ~5%, in good agreement with the observed discontinuity depths and impedance contrast detected here [*Xu et al.*, 2008]. The intermittency of the observed velocity contrast suggests regional "blobs" of eclogitic materials on the order of 500–1000 km across, perhaps isolated through large material viscosity contrasts and not fully mixed into the mantle [*Naliboff and Kellogg*, 2007]. We cannot fully test the lateral geographic extent and regional occurrence of the 300 km discontinuity, but future seismic studies with new arrays should allow us to quantify to regional presence and further characterize this intermittent seismic discontinuity.

5. Conclusions

[14] The small-scale structure of the 300 km seismic discontinuity is studied using SS and PP precursors recorded by High Lava Plains Seismic Array and EarthScope Transportable Array seismometers. Detailed seismic array analysis of earthquakes from 2005 to 2009 shows reflections from the 300 km discontinuity in isolated regions of the Pacific, with the boundary present beneath the Kurile subduction zone, the Tonga-Fiji region, as well as beneath the Nazca subduction zone at 250–310 km depth with an impedance contrast of 4.7%–5.0%. We used forward modeling of SH wave propagation to quantify the detectability of the 300 km seismic discontinuity, finding a laterally varying boundary spanning scale lengths of several 100 kilometers is detectable at short periods (~10 s) although the impedance contrast is underestimated for structures less than 500–750 km in width. We associated the intermittent presence of the 300 km discontinuity with the presence of eclogitic materials in the upper mantle.

[15] **Acknowledgments.** The authors thank two anonymous reviewers and the editor, Michael Wysession, for constructive comments that helped to improve the quality of the manuscript. Data were collected with Standing Order for Data [*Owens et al.*, 2004] and EMERALD [*West and Fouch*, 2012] software. Data analyses were performed using TauP [*Crotwell et al.*, 1999] and Seismic Analysis Code [*Goldstein et al.*, 2003]. Figures were generated using GMT [*Wessel and Smith*, 1998]. NS was supported by a NASA Postdoctoral Program Fellowship. BK was supported by the Carnegie Institution of Washington Summer Scholars Program. The authors gratefully acknowledge the University of Utah Center for High Performance Computing (CHPC) for computer resources and support. MT was partially supported by the National Science Foundation (grant no. EAR-0952187).

References

Akaogi, M., and S. I. Akimoto (1980), High-pressure stability of a dense hydrous magnesian silicate Mg23Si8O42H6 and some geophysical implications, *J. Geophys. Res.*, *85*(NB12), 6944–6948.

Bagley, B., and J. Revenaugh (2008), Upper mantle seismic shear discontinuities of the Pacific, *J. Geophys. Res.*, *113*(B12).

Bagley, B., A. M. Courtier, and J. Revenaugh (2009), Melting in the deep upper mantle oceanward of the Honshu slab, *Phys. Earth Planet. Inter.*, *175*(3–4), 137–144.

Bassin, C., G. Laske, and G. Masters (2000), The current limits of resolution for surface wave tomography in North America, *Eos Trans. AGU*, *81*(48), Fall Meeting Suppl., Abstract S12A-03.

Chaljub, E., and A. Tarantola (1997), Sensitivity of SS precursors to topography on the upper-mantle 660-km discontinuity, *Geophys. Res. Lett.*, *24*(21), 2613–2616.

Courtier, A. M., B. Bagley, and J. Revenaugh (2007), Whole mantle discontinuity structure beneath Hawaii, *Geophys. Res. Lett.*, *34*(17), L17304, doi:10.1029/2007GL031006.

Crotwell, H. P., T. J. Owens, and J. Ritsema (1999), The TauP toolkit: Flexible seismic travel-time and ray-path utilities, *Seismol. Res. Lett.*, *70*, 154–160.

Davies, D., E. J. Kelly, and J. R. Filson (1971), Vespa process for analysis of seismic signals, *Nature-Physical Science*, *232*(27), 8–13.

Deuss, A. (2009), Global observations of mantle discontinuities using SS and PP precursors, *Surv. Geophys.*, *30*(4–5), 301–326.

Deuss, A., and J. H. Woodhouse (2002), A systematic search for mantle discontinuities using SS-precursors, *Geophys. Res. Lett.*, *29*(8), 1249, doi:10.1029/2002GL014768.

Dziewonski, A. M., and D. L. Anderson (1981), Preliminary Reference Earth Model, *Phys. Earth Planet. Inter.*, *25*(4), 297–356.

Efron, B., and R. Tibshirani (1986), Bootstrap methods for standard errors, confidence intervals, and other measures of statistical accuracy, *Statist. Sci.*, *1*(1), 54–75.

Fuchs, K., and G. Müller (1971), Computation of synthetic seismograms with the reflectivity method and comparison with observations, *Geophys. J. R. Astr. Soc.*, *23*, 417–433.

Goldstein, P., D. Dodge, M. Firpo, and L. Minner (2003), SAC2000: Signal processing and analysis tools for seismologists and engineers, in *The IASPEI International Handbook of Earthquake and Engineering Seismology*, edited by W. H. K. Lee, H. Kanamori, P. C. Jennings, and C. Kisslinger, Academic Press, London.

Jahnke, G., M. S. Thorne, A. Cochard, and H. Igel (2008), Global SH-wave propagation using a parallel axi-symmetric spherical finite-difference scheme: application to whole mantle scattering, *Geophys. J. Int.*, doi: 10.1111/j.1365-1246X.2008.03744.x.

Kennett, B. L. N., E. R. Engdahl, and R. Buland (1995), Constraints on seismic velocities in the earth from travel times, *Geophys. J. Int.*, *122*, 108–124.

Li, C., R. D. van der Hilst, E. R. Engdahl, and S. Burdick (2008), A new global model for *P* wave speed variations in Earth's mantle, *Geochem. Geophys. Geosyst.*, *9*, Q05018, doi:10.1029/2007GC001806.

Liu, J., L. Topor, J. Zhang, A. Navrotsky, and R. C. Liebermann (1996), Calorimetric study of the coesite stishovite transformation and calculation of the phase boundary, *Phys. Chem. Min.*, *23*(1), 11–16.

Naliboff, J. B., and L. H. Kellogg (2007), Can large increases in viscosity and thermal conductivity preserve large-scale heterogeneity in the mantle?, *Phys. Earth Planet. Inter.*, *161*(1–2), 86–102.

Owens, T. J., H. P. Crotwell, C. Groves, and P. Oliver-Paul (2004), SOD: Standing order for data, *Seismol. Res. Lett.*, *75*(4), 515–520.

Revenaugh, J., and T. H. Jordan (1991), Mantle Layering From Scs Reverberations 3. *The Upper Mantle, J. Geophys. Res.*, *96*(B12), 19781–19810.

Ritsema, J., A. Deuss, H. J. van Heijst, and J. H. Woodhouse (2011), S40RTS: a degree-40 shear-velocity model for the mantle from new Rayleigh wave dispersion, teleseismic traveltime and normal-mode splitting function measurements, *Geophys. J. Int.*, *184*(3), 1223–1236.

Rost, S., and C. Thomas (2009), Improving seismic resolution through array processing techniques, *Surv. Geophys.*, *30*(4–5), 271–299.

Schmerr, N., and C. Thomas (2011), Subducted lithosphere beneath the Kuriles from migration of PP precursors, *Earth Planet. Sci. Lett.*, *311*(1–2), 101–111.

Shearer, P. M., and M. P. Flanagan (1999), Seismic velocity and density jumps across the 410- and 660-kilometer discontinuities, *Science*, *285* (5433), 1545–1548.

Shearer, P. M., M. P. Flanagan, and M. A. H. Hedlin (1999), Experiments in migration processing of SS precursor data to image upper mantle discontinuity structure, *J. Geophys. Res.*, *104*(B4), 7229–7242.

Wajeman, N. (1988), Detection of Underside P-Reflections at Mantle Discontinuities by Stacking Broad-Band Data, *Geophys. Res. Lett.*, *15*(7), 669–672.

Wessel, P., and W. H. F. Smith (1998), New, improved version of Generic Mapping Tools released, *EOS Trans AGU*, *79*(47), 579.

West, J. D., and M. J. Fouch (2012), EMERALD: A Web Application for Seismic Event Data Processing, *Seismol. Res. Lett.*, *83*(6), 1061–1067.

Williams, Q., and J. Revenaugh (2005), Ancient subduction, mantle eclogite, and the 300 km seismic discontinuity, *Geology*, *33*(1), 1–4.

Woodland, A. B. (1998), The orthorhombic to high-P monoclinic phase transition in Mg-Fe pyroxenes: Can it produce a seismic discontinuity?, *Geophys. Res. Lett.*, *25*(8), 1241–1244.

Xu, W. B., C. Lithgow-Bertelloni, L. Stixrude, and J. Ritsema (2008), The effect of bulk composition and temperature on mantle seismic structure, *Earth Planet. Sci. Lett.*, *275*(1–2), 70–79.

Zhang, Z., and T. Lay (1993), Investigation of Upper Mantle Discontinuities Near Northwestern Pacific Subduction Zones Using Precursors to SSH, *J. Geophys. Res.*, *98*(B3), 4389–4405.

Zheng, Z., and B. Romanowicz (2012), Do double ‘SS precursors’ mean double discontinuities?, *Geophys. J. Int.*, *191*(3), 1361–1373.

Zheng, Y. C., T. Lay, M. P. Flanagan, and Q. Williams (2007), Pervasive seismic wave reflectivity and metasomatism of the Tonga mantle wedge, *Science*, *316*(5826), 855–859.